ACADEMIA GREEN ENERGY

Research Article
Published: 2024-11-29
https://doi.org/10.20935/AcadEnergy7418

The effect of manufacturing defects and license plate on the energy efficiency of solar vehicles

Burak İpek[1], Mehmet Yıldız[1], Tunahan Akış[2,*], Aytaç Gören[1]

Academic Editor: Amjad Anvari-Moghaddam

Abstract

In recent times, research on the energy efficiency of solar vehicles has gained momentum. A significant component of the mentioned efficiency is the vehicle's resistance to airflow. From this perspective, the aim of this study is to investigate the effect of manufacturing defects on the aerodynamic performance of solar vehicles. An analysis of these manufacturing defects at different vehicle speeds has been conducted. In this study, the SOLARIS 11 (S11) solar vehicle has been analyzed in four scenarios: (i) computer-aided design (CAD) version, (ii) CAD version with manufacturing defects, (iii) with a license plate, and (iv) with both manufacturing defects and a license plate. In addition, these four different scenarios have been evaluated separately for vehicle speeds of 60, 90, and 120 km/h. In conclusion, with manufacturing defects, the variation in power consumption of the solar car increased by an average of 24.55–29.09% according to the ideal CAD model. This increase is found to cause a reduction in the vehicle's range by 18.31–37 km. Power consumption of the vehicle was calculated as 237 W for the CAD model, 246 W for the model that has manufacturing defects, and 309 W for the model that has both manufacturing defects and a license plate at 60 km/h. Similarly, power consumption values are calculated as 1,692, 2,167, and 2,214 W at 120 km/h. Additionally, the increase in power consumption caused by the license plate in the absence of manufacturing defects has been examined as a separate section.

Keywords: *computational fluid dynamics, aerodynamics, energy efficiency, solar car aerodynamics*

Citation: İpek B, Yıldız M, Akış T, Gören A. The effect of manufacturing defects and license plate on the energy efficiency of solar vehicles. *Academia Green Energy* 2024;1. https://doi.org/10.20935/AcadEnergy7418

1. Introduction

Efficiency is one of the most important criteria in vehicles powered by solar energy. When examining the components that contribute to power consumption during solar car challenges, it is well known that aerodynamic drag is the most significant factor [1]. In this study, the aerodynamic analyses of the SOLARIS 11 (S11) solar vehicle that is developed by the Dokuz Eylül University (DEU) SOLARIS team are considered under different conditions, focusing mainly on manufacturing defects. These manufacturing defects are part of the concept of interference drag, a component of aerodynamic resistance [2]. This definition also includes the negative impact of certain accessories used in the vehicle on aerodynamic resistance, such as rearview mirrors and license plates. In 2020, Korkut et al. [1] conducted aerodynamic analyses using computational fluid dynamics (CFD) methods on a solar vehicle developed by their team. They observed a 42% increase in the drag coefficient with the use of mirrors and a 23.72% increase with a rearview camera compared to the accessory-free condition. In their 2021 study, Atienza et al. [3] conducted CFD modeling of a solar-powered vehicle with both enclosed and open wheel configurations. They reported that using an enclosed wheel structure improved vehicle aerodynamics and reduced power consumption by 7.22% [4]. Vinnichenko et al. [5] examined the negative effects of photovoltaic panels on the drag coefficient in solar vehicles using a two-dimensional model, providing insights on the solution methodology. In their studies, they reported that analyses involving the addition of the energy equation to CFD solver take longer to converge compared to analyses conducted solely for aerodynamic purposes. In addition, they found that mechanical improvements made on the vehicle positively impacted its power consumption. Singla et al. [6] analyzed the performance of a solar vehicle by reducing the drag coefficient using CFD methods, evaluating their findings separately for the basic vehicle shape, canopy, and wheel fairings. In their 2015 study, Pacheco et al. [7] conducted an aerodynamic analysis of three- and four-wheeled solar cars used in the World Solar Challenge held in Atacama, Chile. They used the RANS (Reynolds-Averaged Navier-Stokes Equations) turbulence model in their solvers and improved the drag coefficient through shape optimizations in the cockpit area. As a result of these optimizations, they reported that although drag resistance accounted for 90% of the total power consumption, this ratio was reduced to 54%. Bobrowski et al. [3] investigated the impact of an under-mounted battery box on the aerodynamic performance of solar-powered vehicles. Through iterative CFD simulations,

[1]Department of Mechanical Engineering, Faculty of Engineering, Dokuz Eylül University, Buca, Izmir 35160, Turkey.
[2]Electric and Energy Department, İzmir Vocational School, Dokuz Eylül University, Buca, Izmir 35160, Turkey.
*email: tunahan.akis@deu.edu.tr

they found that the battery box installation significantly negatively affected aerodynamic performance. However, due to the necessity of using this battery box, they made efforts for improvement, ultimately achieving a 43% enhancement in the vehicle's aerodynamic performance. Waluo et al. [8] analyzed the effects of a spoiler accessory mounted on a solar-powered vehicle at various attack angles against the airflow. Based on their findings, they reported that optimizing the attack angle could reduce the drag coefficient by 6.96–14.01%. Chitnis et al. [9] conducted CFD analyses of solar-assisted vehicles, creating their models according to the Electric Solar Vehicle Championship (ESVC) 2020 rule book. Their analyses calculated a drag coefficient of 0.697, and they observed that the wake region extended over a larger area compared to other commercial vehicles. Nabil et al. [10] addressed numerical aerodynamic analyses conducted on vehicle bodies in general. Based on his findings, he reported that power consumption related to the drag coefficient is not solely dependent on the frontal area of the vehicle; instead, these analyses should be conducted separately for each vehicle model.

This study addresses the negative effects of manufacturing defects, resulting from the vehicle's exterior shell production method, on power consumption due to aerodynamic drag. The body of the examined vehicle is produced using the vacuum-assisted resin transfer molding (VARTM) method. In this manufacturing process, a vacuum pump is used to direct resin through a porous fabric structure, filling the mold cavity [11, 12]. Once the cavity is filled, the fiber part is removed and assembled onto the solar car body, and finally, the vehicle is manufactured. However, due to the complex assembly nature of the solar car, the VARTM-produced body design contains some manufacturing defects. It is believed that these defects lead to extra energy consumption due to aerodynamic drag while the solar car is in motion. Unlike previous literature, this study creates a numerical model with these manufacturing defects, and the relevant network structure is analyzed in the commercial CFD solver ANSYS-Fluent. By modeling these manufacturing defects, compared to a clean computer-aided design (CAD) model, a more realistic simulation is achieved. CFD analyses have been used since the 1990s to gain a competitive advantage in aerodynamics, especially in racing cars, and today it is one of the most important parts of the automotive industry [13]. In recent years, CFD has been instrumental in numerically defining the flow around vehicles and understanding the behavior of the flow, thereby determining the performance of the vehicle. This study uses CFD simulations to analyze the impact of many manufacturing defects on the S11 solar vehicle model like solar panel offset, wheel intervention covers offset, etc. Four different model analyses are conducted for the S11 car: (1) without surface defects, (2) with surface defects, (3) without surface defects with a license plate installed, (4) and with surface defects and a license plate.

1.1. SOLARIS 11 solar car

The SOLARIS solar car development team was founded in 2003 at Mechanical Engineering Department, DEU. The SOLARIS team is a student-led organization dedicated to designing and producing innovative solar-powered racing vehicles. The team participates in prestigious international competitions, including the Bridgestone World Solar Challenge (BWSC) and the Sasol Solar Challenge. The characteristics of the latest car produced by this team, S11, are given in **Table 1**. In this study, the aerodynamic performance of the final model specified in this section has been analyzed. The S11 model, a solar-assisted vehicle designed and manufactured by the SOLARIS team, is shown in **Figure 1**.

Table 1 • SOLARIS 11 solar car model characteristics

No.	Parameter	Value
1	Vehicle mass (full load)	280 kg
2	Natural frequency	2.5–3.0 Hz
3	Average cruise speed	75 km/h
4	Tire scrub	5 mm
5	Toe angle	0.5° (in)
6	Track width	800 mm
7	Wheelbase	2,200 mm
8	Front instantaneous center height	79.20 mm
9	Rear instantaneous center height	319.51 mm
10	Center of gravity height	200 mm
11	Distance between instantaneous center and front axle	902 mm
12	Perpendicular distance between center of gravity and roll axis	5 mm
13	Camber	1° (negative)

In previous studies by the SOLARIS team (S7 model), the impact of using cameras, instead of mirrors, on power consumption was investigated, concluding that camera usage is more energy-efficient [14]. **Figure 2** illustrates the status of the S11 model compared to the aforementioned findings. As shown in the figure, the power consumption of the S11 model is 14% higher than that of the S7 model, which utilizes cameras instead. This effect will be addressed in future studies, where thermal analyses will also be incorporated into the model solution to more thoroughly assess the energy efficiency of the S11 model.



Figure 1 • SOLARIS 11 solar car.

1.2. Vacuum-assisted resin transfer molding method

Due to manufacturing constraints and the complex geometry of the vehicle, some production defects are inevitable. Composite sandwich panels consist of two thin, high-strength face sheets bonded to a thick, low-density core. The common manufacturing process for these panels is the hand layup method. However, this method relies heavily on operator skill, which can result in inconsistent product quality [15]. In the production of the solar car body, polymer matrix composites have been used in many parts of the body and the vehicle. Reinforcement materials such as carbon fiber, glass fiber, and aramid fabric have been employed, with balsa wood used as the matrix element. The manufacturing method used is the VARTM process. **Figure 3** shows a schematic of the VARTM process. This method requires the preparation of a model mold. Since the preparation of the mold relies on detailed manual labor and human effort, the process has some error rate. Consequently, the primary causes of manufacturing defects can be attributed to deficiencies in craftsmanship or insufficient human effort.

The SOLARIS team constructs a solar car using their own resources within the university. They create foam molds for the design tools and manufacture the components using the VARTM method. The two stages of using this method in the production of the solar vehicle are illustrated in **Figure 4**.

Surface defects caused by production may cause unwanted turbulence on the vehicle. Manufacturing defects such as panel and surface irregularities can disrupt airflow and increase friction, resulting in greater energy consumption and lower distance range and speed. A common manufacturing defect of most solar cars, including the S11, is irregularities on the solar panel surface.

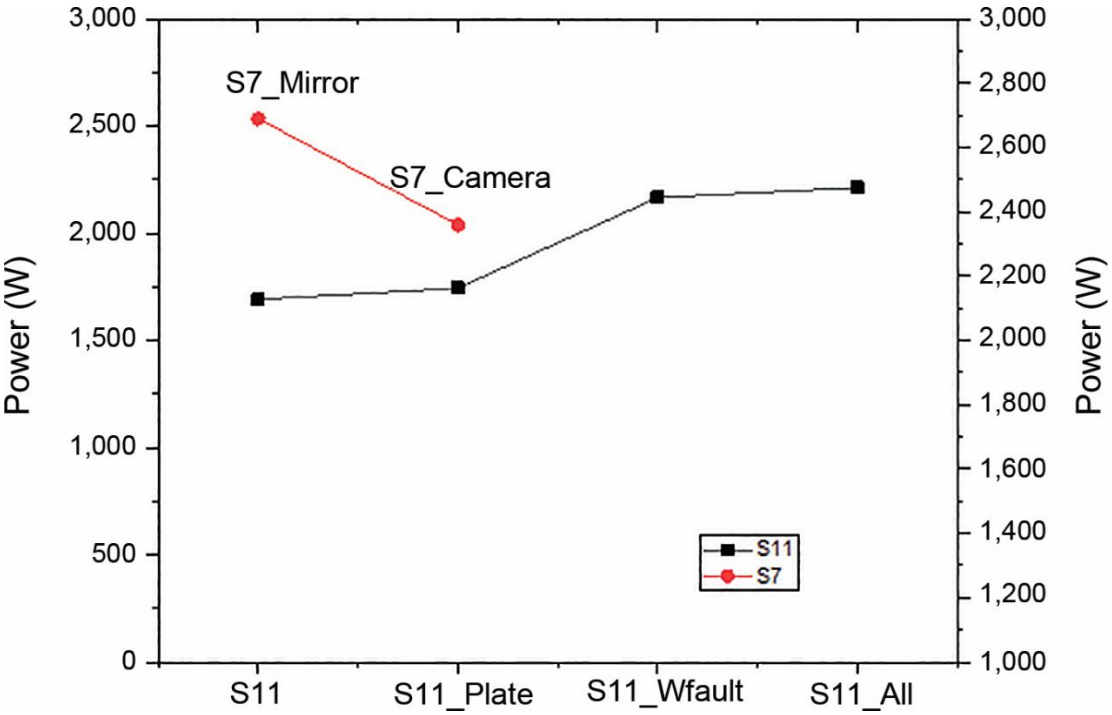


Figure 2 • Comparison energy efficiency with old S7 model of the SOLARIS team.

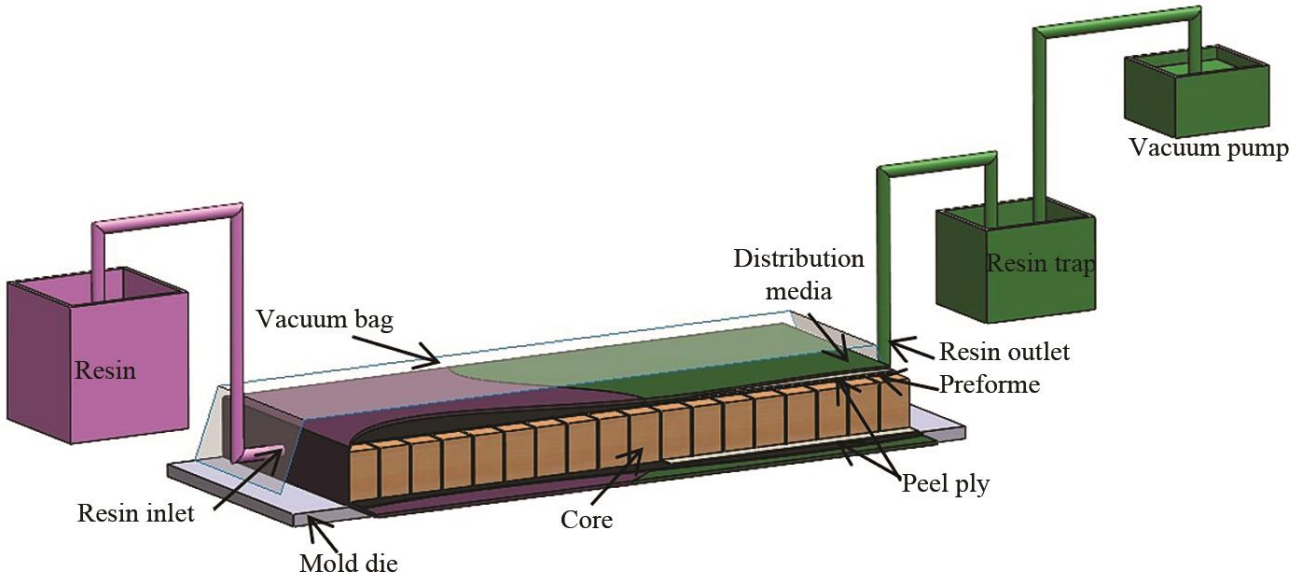


Figure 3 • Schematic of the vacuum-assisted resin transfer molding method.



Figure 4 • SOLARIS 11 manufacturing stages.

2. Problem definition and boundary conditions

The manufacturing and assembly of solar vehicle, as well as the development of a computational model for aerodynamic analyses, are created using the commercial design software SOLIDWORKS. Dimensions of solar vehicle and numerical wind tunnel are given in **Table 2**. The boundary conditions of the computational domain are shown in **Figure 5**. The boundary conditions of the problem, according to **Figure 4**, are provided in **Table 3**.

The body of the vehicle and sidewalls are designated as stationary walls with the no-slip shear condition. The entrance of the computational domain is defined as a velocity inlet, while the outlet section is defined as a pressure outlet with a gauge pressure of 0 Pa. The types and numerical values of boundary conditions are summarized in **Table 4**.

Table 2 • Model and wind tunnel dimensions

	Length (m)	Width (m)	Height (m)
SOLARIS 11	5	1.385	1.085
Wind tunnel	50	7.62	6.085

Table 3 • Standard sea level values for the free stream properties

Pressure	Density	Temperature	Kinematic viscosity
101.325 Pa	1.2250 kg/m^3	288.16 K	1.4607e-5 m^2/s

Table 4 • Types of boundary conditions and values

Boundary	Boundary type	Value
Inlet	Velocity inlet	25 m/s
Outlet	Pressure outlet	0 Pa
Vehicle surface	Stationary wall	No slip
Wall	Stationary wall	No slip

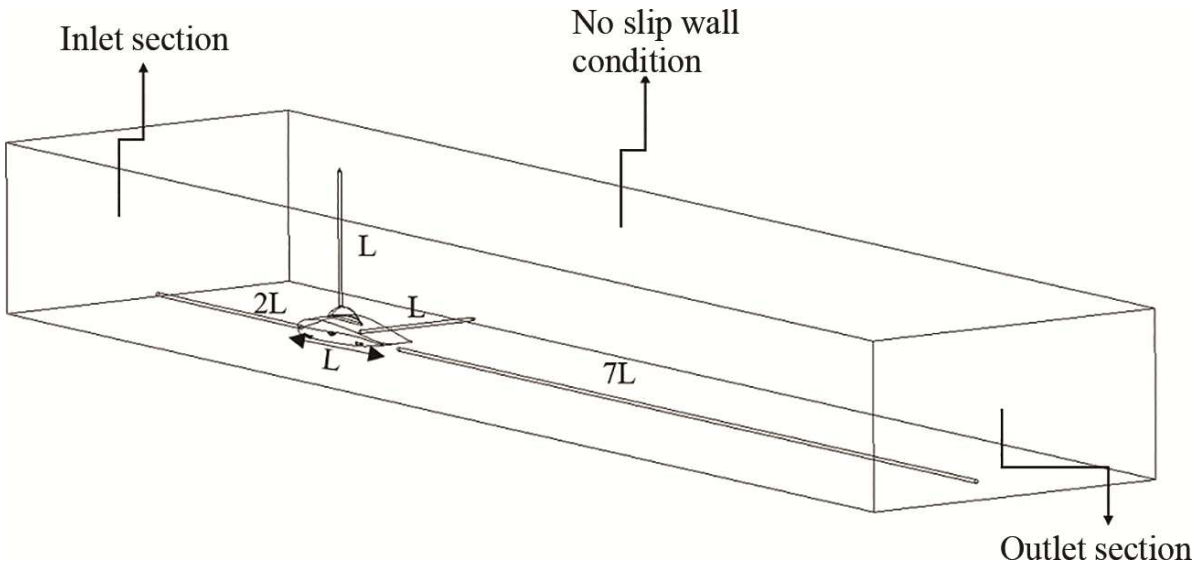


Figure 5 • Computational domain.

3. Solution method

In this study, a numerical model is obtained by subtracting the volume of S11 solar car model, whose aerodynamic performance is to be examined in a numerical wind tunnel. First, the model is divided into finite volumes (meshing) and solved using the coupled algorithm. Second-order upwind discretization is implemented on conservation equations. The necessary governing equations for this analysis are given in Eq. (1) (mass conservation), Eq. (2) (x-momentum), Eq. (3) (y-momentum), and Eq. (4) (z-momentum) [16]. Equation (1) is mass conservation, where the u term represents the velocity in the x-direction, the v term represents the velocity in the y-direction, and the w term represents the velocity in the z-direction. In addition, the k-omega (k–ω) turbulence model is used to visualize and capture turbulence in the wind tunnel. The k-omega (k–ω) turbulence model is one of the most commonly used models [17, 18] for capturing the effects of turbulent flow conditions. Equations (2–4) are momentum conservation terms in the x-, y-, and z-directions, respectively.

$$\frac{\partial(\rho u)}{\partial x}+\frac{\partial(\rho v)}{\partial y}+\frac{\partial(\rho w)}{\partial z}=0 \quad (1)$$

$$\rho\left(u\frac{\partial u}{\partial x}+v\frac{\partial u}{\partial y}+w\frac{\partial u}{\partial y}\right)=\rho gx-\frac{\partial P}{\partial x}+\frac{\partial}{\partial x}\left(2\mu\frac{\partial u}{\partial x}+\lambda\vec{\nabla}.\vec{V}\right)+\frac{\partial}{\partial y}\left[\mu\left(\frac{\partial u}{\partial y}+\frac{\partial v}{\partial x}\right)\right]+\frac{\partial}{\partial z}\left[\mu\left(\frac{\partial w}{\partial z}+\frac{\partial u}{\partial z}\right)\right] \quad (2)$$

$$\rho\left(u\frac{\partial v}{\partial x}+v\frac{\partial v}{\partial y}+w\frac{\partial v}{\partial z}\right)=\rho gy-\frac{\partial P}{\partial y}+\frac{\partial}{\partial x}\left[\mu\left(\frac{\partial v}{\partial x}+\frac{\partial u}{\partial y}\right)\right]+\frac{\partial}{\partial y}\left[2\mu\left(\frac{\partial v}{\partial y}+\lambda\vec{\nabla}.\vec{V}\right)\right]+\frac{\partial}{\partial z}\left[\mu\left(\frac{\partial v}{\partial z}+\frac{\partial uw}{\partial z}\right)\right] \quad (3)$$

$$\rho\left(u\frac{\partial w}{\partial x}+v\frac{\partial w}{\partial y}+w\frac{\partial w}{\partial y}\right)=\rho gz-\frac{\partial P}{\partial z}+\frac{\partial}{\partial x}\left[\mu\left(\frac{\partial w}{\partial x}+\frac{\partial u}{\partial z}\right)\right]+\frac{\partial}{\partial y}\left[\mu\left(\frac{\partial v}{\partial z}+\frac{\partial w}{\partial y}\right)\right]+\frac{\partial}{\partial z}\left[2\mu\left(\frac{\partial w}{\partial z}+\lambda\vec{\nabla}.\vec{V}\right)\right] \quad (4)$$

The shear-stress transport (SST) k–ω turbulence model, proposed by Menter in 1993, stands as a widely embraced two-equation eddy-viscosity model [19]. This formulation, known as SST, harmoniously merges two advantageous approaches. Specifically, the use of a k–ω formulation within the inner regions of the boundary layer makes the model directly applicable throughout the entire boundary layer, extending seamlessly down to the wall through the viscous sublayer. Consequently, the SST k–ω model proves versatile, serving as a Low-Re turbulence model without the need for additional damping functions [14, 20]. The three-dimensional incompressible turbulent flow over the solar vehicle is simulated with Reynolds-averaged Navier–Stokes equations using the commercial finite volume solver package ANSYS-Fluent v23.2. Moreover, Menter's [20] k–ω SST turbulence model is used to account for the turbulence effect on the numerical simulations. The following assumptions are made in the analyses:

- Flow is incompressible
- Air properties are ideal
- Steady state flow regime

Under these assumptions and methods, 20 different parametric analyses are conducted, and the results of the analyses are presented in the results section.

4. Mesh structure

This section focuses on mesh independence, aiming to determine the optimum structure and solving time. The most accurate results are obtained with a 25 mm mesh size. *Tetrahedron meshes are used for simulations for both the air domain and the inflated boundary layer*. However, for optimal solving time and enhanced accuracy, the structure with a 15 mm mesh size is identified.

An image of the meshed model is shown in **Figure 6**. As shown in the figure, the mesh refinement process is applied to the surfaces of the vehicle in contact with air, aiming to improve the model for problem convergence.

In addition, the sufficiency of finite volumes is examined in relation to the drag coefficient. The results of this analysis are presented in **Figure 7**, where it is observed that the analysis is independent of mesh count, with 8 million nodes (highlighted by the red frame) deemed sufficient.

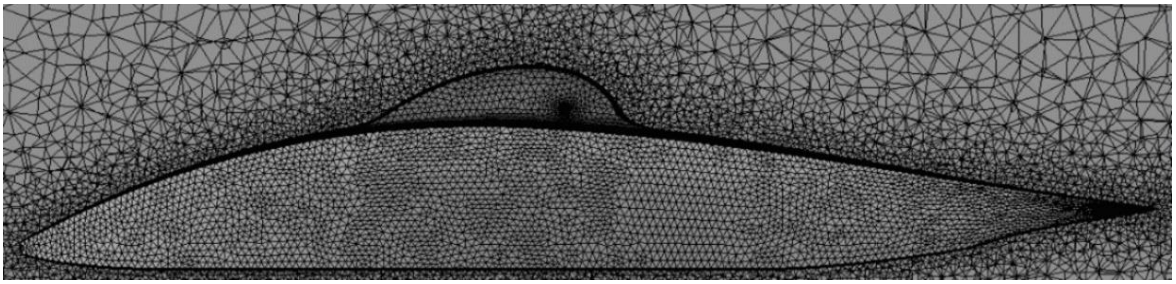


Figure 6 • Mesh model.

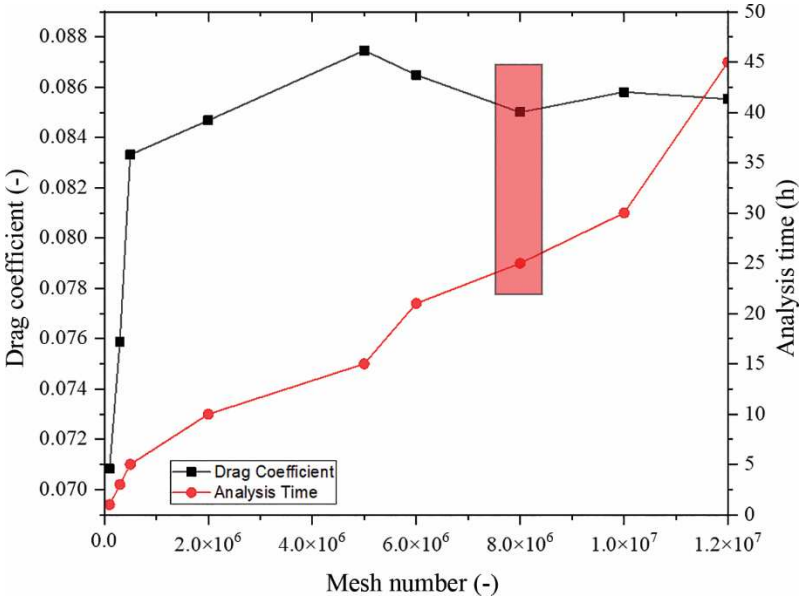


Figure 7 • Validation of drag coefficients and time periods of analyses depending on the finite volume number.

5. Results

5.1. Analysis of the SOLARIS 11 computer-aided design model

In this section, the aerodynamic component of power consumption of the S11 is analyzed using its CAD version. These values are examined as the foundation, as efficiency-based races typically involve average speeds of 60–90 km/h. In addition, 120 km/h is considered to avoid encountering maximum aerodynamic forces.

The design model of the S11 vehicle is depicted in **Figure 8**, and the calculated power consumption according to the drag coefficient is given in **Table 5**.

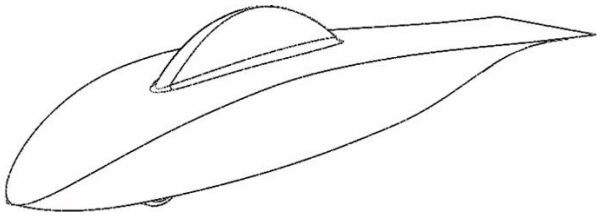


Figure 8 • SOLARIS 11 computer-aided design model isometric view.

Table 5 • SOLARIS 11 Cd, CdA, and power values for specific speeds

Vehicle	Frontal area: 0.92 m²	Speed (km/h)		
	Parameter	60	90	120
SOLARIS 11	Cd	0.09074	0.08488	0.082
	CdA	0.08348	0.078089	0.07462
	Power (W)	237	747	1,692

In **Figure 9**, the analysis focuses solely on the CAD model, displaying the static pressure distribution across the vehicle. As expected, a low-pressure zone has formed at the top of the vehicle canopy, creating flow separation just behind the driver cockpit (at nearly x = 0.8 m coordinate). Under these conditions, the power consumption of the vehicle has been calculated as 237 W at 60 km/h, 747 W at 90 km/h, and 1,692 W at 120 km/h.

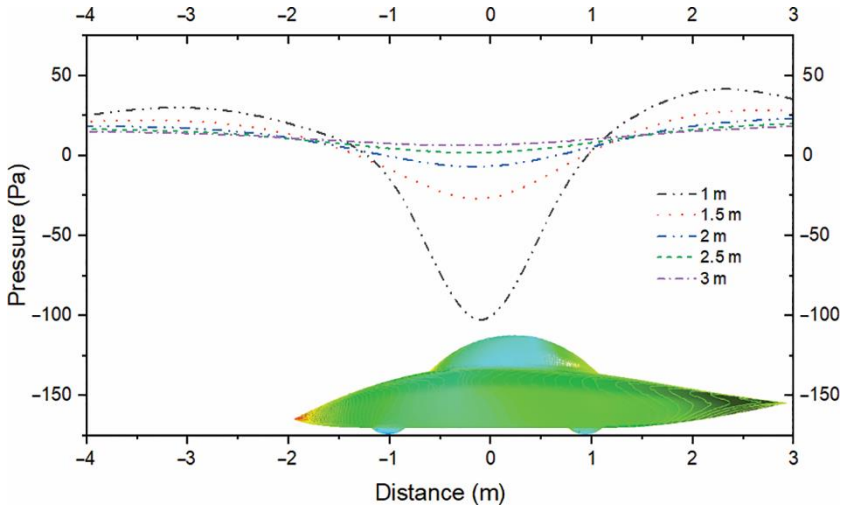


Figure 9 • The pressure distribution observed on the center plane of SOLARIS 11 solar car.

5.2. Analysis of the SOLARIS 11 model with manufacturing defects

Manufacturing defects shown in **Figure 10** are modeled on the numerical model, and the analysis is conducted with the same inputs as the initial model to obtain more realistic results. The results are summarized in **Table 6**. In **Figure 9**(b–d), you can observe the 10 mm protrusion caused by the panels, the 3 mm protrusion caused by the wheel intervention covers not being seated, the 10 mm protrusion caused by the surface irregularity at the front of the canopy, and the external emergency button and the protrusion caused by the cooler block of the rear LEDs.

In **Figure 11**, the analysis focuses on the model with manufacturing defects, displaying the static pressure distribution across the vehicle. As expected, a low-pressure zone has formed at the top of the vehicle canopy, but manufacturing defects have caused the vacuum zone to shift toward the front surface (at nearly $x = -0.2$ m coordinate) of the vehicle, leading to an increase in the drag coefficient value and flow separation just behind the driver cockpit. Under these conditions, the power consumption of the vehicle has been calculated as 295 W at 60 km/h, 945 W at 90 km/h, and 2,167 W at 120 km/h, as shown in **Table 5**.

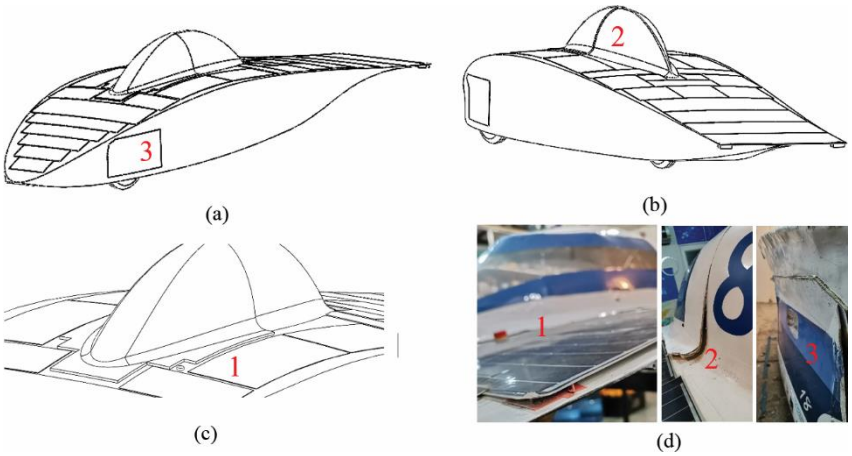


Figure 10 • SOLARIS 11 manufacturing defects: (a) frontal view, (b) back view, (c) detailed driver cockpit, and (d) real view of defects.

Table 6 • S11_wfault Cd, CdA, and power values for specific speeds

Vehicle	Frontal area: 0.93 m²	Speed (km/h)		
	Parameter	60	90	120
SOLARIS 11 with defects	Cd	0.1118	0.10622	0.10275
	CdA	0.103974	0.098785	0.09555
	Power (W)	295	945	2,167

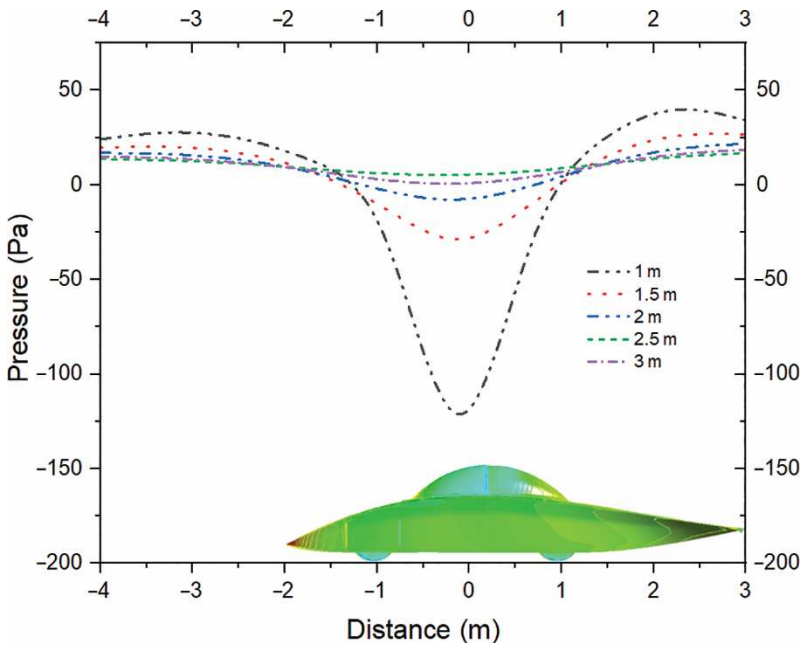


Figure 11 • The pressure distribution observed on the center plane.

5.3. Computational fluid dynamics analysis of the SOLARIS 11 model with a license plate

The BWSC is held on Stuart Highway in Australia. According to World Solar Challenge (WSC) regulations, for a solar car to participate in the race, it must pass static and dynamic inspections and have a license plate [21]. To ensure that the integration of the license plate does not significantly increase the aerodynamic drag coefficient, a design where the license plate carrier is seamlessly integrated with the vehicle body has been implemented. In **Figure 12**, the location of the license plate on the solar car can be seen. In this section, without considering manufacturing defects, the investigation focuses solely on the CAD geometry to analyze the change in drag coefficient with the addition of a license plate. Results are summarized in **Table 7**.

In **Figure 13**, the analysis focuses on the model with a license plate, displaying the static pressure distribution across the vehicle. As expected, a low-pressure zone has formed at the top of the vehicle canopy, but the license plate has caused the vacuum zone to move toward the front surface (at nearly x = −0.07 m coordinate) of the vehicle, leading to an increase in the drag coefficient value and flow separation just behind the driver cockpit. Under these conditions, the power consumption of the vehicle has been calculated as 246 W at 60 km/h, 777 W at 90 km/h, and 1,745 W at 120 km/h, as shown in **Table 6**. If the license plate is positioned considering the airflow direction and pressure distribution on the vehicle, it is evident that integrating the plate on the vehicle does not cause a significant increase in power consumption as much as manufacturing errors.

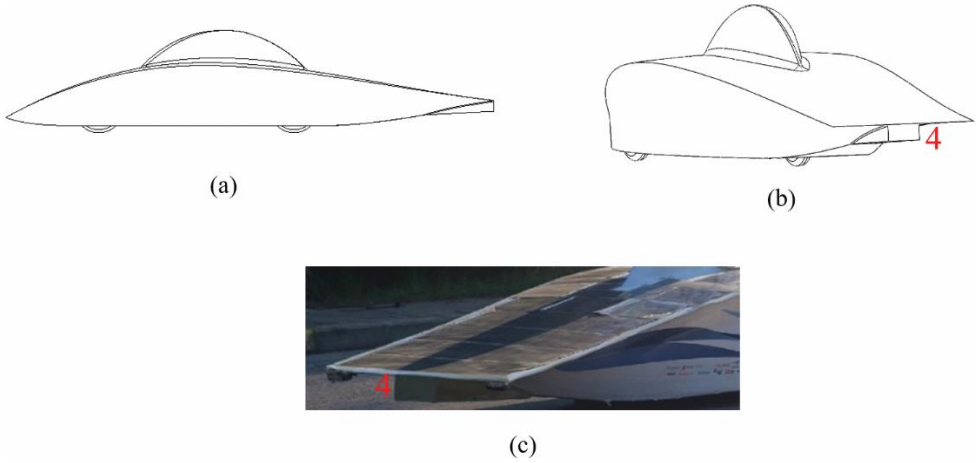


Figure 12 • SOLARIS 11 with a license plate: (a) side view, (b) front view (indicated with 4), and (c) real view.

Table 7 • SOLARIS 11 with license plate Cd, Cd*A, and power values for specific speeds

Vehicle	Frontal area: 0.92 m²	Speed (km/h)		
	Parameter	60	90	120
SOLARIS 11 with a plate	Cd	0.0951	0.08828	0.08362
	CdA	0.08749	0.0812	0.0769304
	Power (W)	246	777	1,745

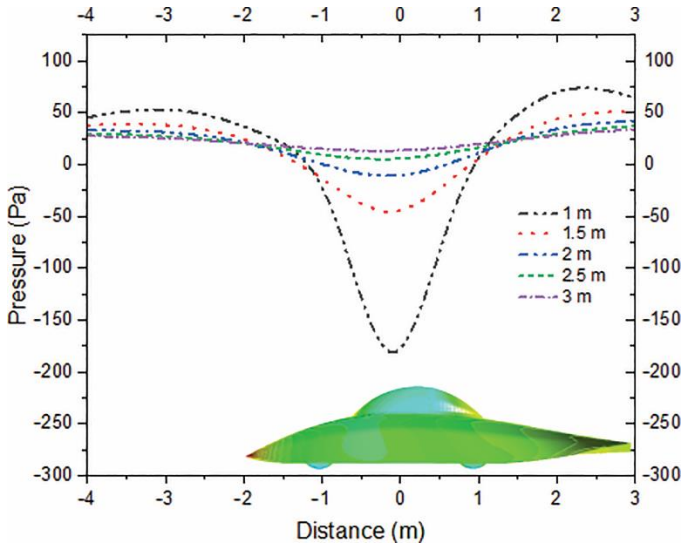


Figure 13 • SOLARIS 11 with a license plate: the pressure distribution observed on the center plane.

5.4. Analysis of the SOLARIS 11 model with manufacturing defects and a license plate

In this section, a license plate is added to the model with manufacturing defects, representing the most realistic version of the actual S11 vehicle, as shown in **Figure 14**. The results are summarized in **Table 8**.

In **Figure 15**, the analysis focuses on a model with both a license plate and manufacturing defects, displaying the static pressure distribution across the vehicle. As expected, a low-pressure zone has formed at the top of the vehicle canopy, but compared to previous results, the integration of the license plate with production errors has resulted in a greater increase in power consumption, leading to a higher drag coefficient value and flow separation just behind the driver cockpit. Under these conditions, the power consumption of the vehicle has been calculated as 309 W at 60 km/h, 965 W at 90 km/h, and 2,214 W at 120 km/h, as shown in **Table 7**.

The calculated drag coefficients and power values for the three different scenarios are presented in **Figure 16** for comparison. In **Figure 16**(a), the drag coefficient is shown according to varying vehicle speeds for the analyzed models: the baseline CAD model S11, the model considering only manufacturing defects (S11_wfault), and the model created by adding only the license plate (S11_plate). In contrast, **Figure 16**(b) presents the power consumption values. As shown in **Figure 16**(a), adding manufacturing defects to the baseline CAD model resulted in an increase in the drag coefficient by 23% at 60 km/h, 30% at 90 km/h, and 25% at 120 km/h. In **Figure 16**(b), power consumption from an aerodynamic perspective showed increases of 24% at 60 km/h, 27% at 90 km/h, and 28% at 120 km/h. Similarly, adding only the license plate caused the drag coefficient to increase by 4% at 60 km/h, 4% at 90 km/h, and 3% at 120 km/h. From an aerodynamic perspective, power consumption increased by 5% at 60 km/h, 6% at 90 km/h, and 2% at 120 km/h.

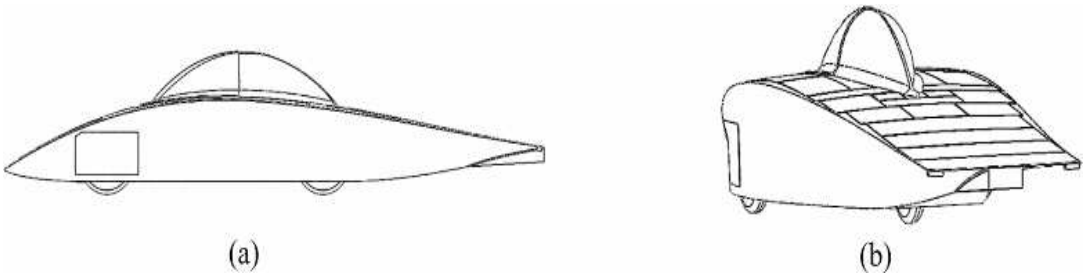


Figure 14 • SOLARIS 11 with a license plate and manufacturing defects: (a) side view and (b) back view.

Table 8 • S11_all Cd, CdA, and power values for specific speeds

Vehicle	Frontal area: 0.93 m²	Speed (km/h)		
	Parameter	60	90	120
SOLARIS 11 with defects and a plate	Cd	0.11643	0.108396	0.10498
	CdA	0.1092799	0.1008083	0.0976314
	Power (W)	309	965	2,214

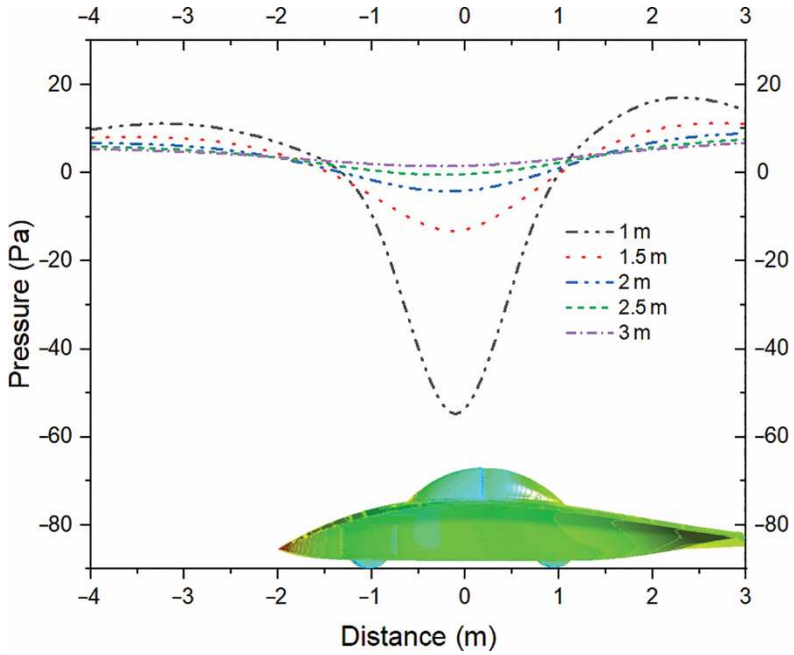


Figure 15 • SOLARIS 11 with a license plate and manufacturing defects: the pressure distribution observed on the center plane.

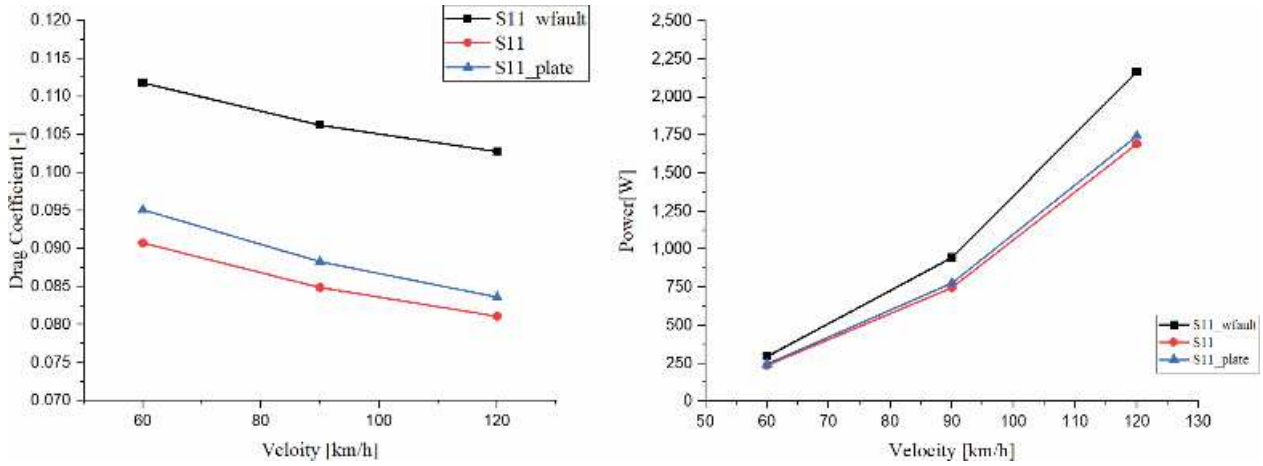


Figure 16 • Results for SOLARIS 11 model and SOLARIS 11 with manufacturing defects: (a) drag coefficient and (b) power consumption.

6. Conclusions

- As a result of this study, it is observed that manufacturing defects arising from the commonly used VARTM production method for solar-powered cars [12], as well as the addition of a vehicle license plate mandated by the new race regulations [21], have significant impacts on the aerodynamic performance of solar-powered vehicles. The key findings of the study can be summarized as follows: an increase in drag coefficient can be attributed to a 1.087% enlargement in the frontal area due to surface defects and heightened turbulence caused by these defects.
- When only manufacturing defects are added to the baseline CAD model, the vehicle's drag coefficient increased by 23% at a speed of 60 km/h, 30% at 90 km/h, and 25% at 120 km/h. In terms of power consumption, increases of 24% at 60 km/h, 27% at 90 km/h, and 28% at 120 km/h are observed. When only the license plate is added to the baseline CAD model, the vehicle's drag coefficient increased by 4% at a speed of 60 km/h, 4% at 90 km/h, and 3% at 120 km/h. In terms of power consumption, increases of 5% at 60 km/h, 6% at 90 km/h, and 2% at 120 km/h are observed.
- When both manufacturing defects and the license plate are added to the baseline CAD model, the vehicle's drag coefficient increased by 28% at a speed of 60 km/h, 28% at 90 km/h, and 22% at 120 km/h. In terms of power consumption, increases of 30% at 60 km/h, 29% at 90 km/h, and 31% at 120 km/h were observed.

As evidenced by these results, CFD analyses are crucial in the development of solar-powered vehicles. Manufacturing errors, which are inevitable, significantly impact the vehicle's projected performance compared to the ideal design. Therefore, whenever major revisions are required during vehicle production, aerodynamic analyses must be conducted. The observed data trends align with studies (e.g., [22, 15]) conducted on this topic. Comparatively, it is evident that each model developed by the SOLARIS team has improved aerodynamic performance and produced more energy-efficient vehicles for competition.

Funding

The authors declare no financial support for the research, authorship, or publication of this article.

Author contributions

Conceptualization, B.I. and M.Y.; methodology, B.İ.; software, B.İ.; validation, B.İ. and M.Y.; formal analysis, B.İ.; investigation, B.İ.; resources, M.Y.; data curation, B.İ.; writing—original draft preparation, B.İ.; writing—review and editing, T.A.; visualization, T.A.; supervision, A.G.; project administration, A.G. All authors have read and agreed to the published version of the manuscript.

Conflict of interest

The authors declare no conflict of interest.

Data availability statement

Data supporting these findings are available within the article, at https://doi.org/10.20935/AcadEnergy7418, or upon request.

Institutional review board statement

Not applicable.

Informed consent statement

Not applicable.

Additional information

Received: 2024-08-06

Accepted: 2024-11-07

Published: 2024-11-29

Academia Green Energy papers should be cited as *Academia Green Energy 2024*, ISSN 2998-3665, https://doi.org/10.20935/

AcadEnergy7418. The journal's official abbreviation is *Acad. Energy*.

Publisher's note

Academia.edu Journals stays neutral with regard to jurisdictional claims in published maps and institutional affiliations. All claims expressed in this article are solely those of the authors and do not necessarily represent those of their affiliated organizations, or those of the publisher, the editors, and the reviewers. Any product that may be evaluated in this article, or claim that may be made by its manufacturer, is not guaranteed or endorsed by the publisher.

Copyright

© 2024 copyright by the authors. This article is an open access article distributed under the terms and conditions of the Creative Commons Attribution (CC BY) license (https://creativecommons.org/licenses/by/4.0/).

References

1. Korkut TB, Goren A, Ezan MA. A CFD study on photovoltaic performance investigation of a solar racing car. In Environmentally-benign energy solutions.Cham: Springer International Publishing; 2020. p. 509–29.
2. Jones B. Elements of practical aerodynamics. 3rd ed. New York: Wiley; 1942.
3. Bobrowski J, Sobczak K. Numerical investigations on the effect of an underbody battery on solar vehicle aerodynamics. Arch Thermodyn. 2021;42:247–60. doi: 10.24425/ather. 2021.139661
4. Wickström R, Moreno Atienza T. Utveckling av hjulinkapsling till JU Solar Team: undersökning av flöde på inkapslade hjul i en solcellsdriven bilkaross. Uppsala: DiVA, Uppsala University; 2021.
5. Vinnichenko NA, Uvarov AV, Znamenskaya IA, Ay H, Wang TH. Solar car aerodynamic design for optimal cooling and high efficiency. Solar Energy. 2014;103:183–90. doi: 10.1016/j.solener.2014.02.019
6. Singla D, Tayal A, Sharma R, Kesari D. Aerodynamic development of a solar car. Int J Eng Res Technol. 2015;4(6):371–6.
7. Pacheco P, Garrido D, Moraga N, Abarcia A. Aerodynamic design of solar energy cars for Australian and Chilean race competitions. La Serena: University of La Serena; 2015.
8. Waluyo J, Hariyanto SD, Lestari N. Evaluation of spoiler design on the aerodynamic performance of an energy-efficient car prototype body. Eng Technol J. 2024;9:4972–7. doi: 10.47191/etj/v9i08.49
9. Chitnis T, Borkar N, Kumawat S, Adepu V. Aerodynamic design and development of Infiniti 4.0 solar car using CFD. Int J Eng Res Technol. 2020;9:527–32. doi: 10.17577/IJERTV9IS030528
10. Nabil T, Helmy Omar AB, Mohamed Mansour T. Experimental approach and CFD simulation of battery electric vehicle body. Int J Fluid Mech Thermal Sci. 2020;6(2):36. doi: 10.11648/j.ijfmts.20200602.11
11. Senan M. Monitoring of part dimensions and fiber content in Vacuum Assisted Resin Transfer Molding (VARTM) process [Doctoral dissertation]. İstanbul: Koç University; 2007.
12. Gören A, Atas C. Manufacturing of polymer matrix composites using vacuum assisted resin infusion molding. Arch Mater Sci Eng. 2008;34(2):117–20. Urlich's Periodical Directory.
13. Marvin JG. Perspective on computational fluid dynamics validation. AIAA J. 1995;33(10):1780–6. Dryden lectureship in research. doi: 10.2514/3.12727
14. Korkut TB, Goren A. Aerodynamic effect of wing mirror usage on the Solaris 7 solar car and Demobil 09 electric vehicle. Int J Automot Mech Eng. 2020;17(2):7868–81. doi: 10.15282/ijame.17.2.2020.06.0587
15. Halimi F, Golzar M, Asadi P, Beheshty MH. Core modifications of sandwich panels fabricated by vacuum-assisted resin transfer molding. J Compos Mater. 2013;47(15):1853–63. doi: 10.1177/0021998312451763
16. Fluent A. 12.0/12.1 Documentation. ANSYS; 2009.
17. Gören A. Solar energy harvesting in electro mobility. Energy harvesting and energy efficiency. Cham, Switzerland: Springer International Publishing AG; 2017. p. 293–326.
18. Keith Hanna R. CFD in sport - a retrospective, 1992–2012. Procedia Engineering. Vol. 34; 2012. p. 622–7. ISSN: 1877-7058. doi: 10.1016/j.proeng.2012.04.106
19. Menter FR. Zonal two equation k–ω turbulence models for aerodynamic flows. AIAA Paper 93-2906; 1993.
20. Menter FR. Two-equation eddy-viscosity turbulence models for engineering applications. AIAA J. 1994;32(8):1598–605. doi: 10.2514/3.12149
21. Regulations Version 2.0 for the 2023 Bridgestone World Solar Challenge. [cited 2024 Nov 19]. Available from: https://www.bridgestone.com/bwsc/about/regulations.html
22. Khan RS, Umale S. CFD aerodynamic analysis of Ahmed body. Int J Eng Trends Technol. 2014;18(7):301–8. doi: 10.14445/22315381/IJETT-V18P262